Interpretable Spectra PCA for Condition Monitoring of Rotating Machinery: Theoretical and Experimental Investigations

Yingchun Li, Yu Sun, *Member, IEEE*, Zhiyuan Li, Xuefeng Chen, *Senior Member, IEEE*, and Laihao Yang, *Member, IEEE*

***Abstract*— Condition monitoring (CM) of rotating machinery is crucial for condition-based maintenance (CBM), ensuring safety and timely fault detection. Principal component analysis (PCA), an unsupervised learning algorithm for data dimensionality reduction, is widely employed for feature extraction in CM. In contrast to typical applications where PCA serves as a data preprocessing tool, this article proposes a novel approach that links principal components (PCs) obtained through PCA dimensionality reduction of degraded data spectra with a data fusion level health indicator (HI). The approach elucidates the physical significance and changing patterns of these PCs in the frequency domain. Notably, the second PC-based Fourier spectrum (PCBFS-2) effectively discriminates between normal and fault frequencies, enabling automated fault feature recognition. The effectiveness of this method in CM and fault feature recognition is validated through simulations and experiments. Importantly, this approach is interpretable, offering a new perspective for combining data-driven modeling with machine learning techniques.**

***Index Terms*— Health indicator (HI), machine condition monitoring (CM), principal component analysis (PCA), spectral amplitudes.**

I. Introduction

PROGNOSITIC and health management (PHM) of mechanical equipment has gained increasing importance in recent years due to their ability to predict and mitigate potential future system risks, minimize maintenance expenses, and enhance mission success [1], [2], [3]. PHM primarily focuses on condition monitoring (CM), fault diagnosis, and predicting the remaining useful life (RUL) of mechanical equipment throughout its lifetime [4], [5]. Among them, CM [6], [7], [8], as the first phase and a crucial component of condition-based maintenance (CBM) [9], aims to extract useful features from the raw signals (such as vibration signals and acoustic signals) to monitor the health condition of the machine and continually track the fault degradation. This process can provide effective information for the subsequent classification of the failure modes classification and RUL prediction.

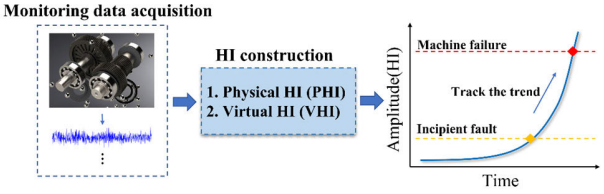

Fig. 1. CM and HI construction applications.

A. Related Works and Motivation

As shown in Fig. 1, a common strategy used in CM is to construct an appropriate health indicator (HI) and then use this HI to monitor the machine's state, enabling early fault detection and degradation process assessment. Depending on their construction strategy, HIs are usually categorized into two types: physics HIs (PHIs) and virtual HIs (VHIs) [10], [11]. PHIs typically use statistical methods and signal processing methods to quantify the energy of the signal or the fault-related characteristics of the signal. As basic statistical indicators, the root mean square (rms) and kurtosis are the most commonly employed PHIs for CM and RUL prediction. Li et al. [12] utilized kurtosis to identify the first predicting time (FPT) and employed rms as the predictive index for bearing RUL prediction. Malhi et al. [13] extracted rms and peak values from the wavelet coefficients as a signal preprocessing technique to predict the RUL of bearings. Despite the ease of calculating these statistical indicators, they are less sensitive to some failure characteristics. For instance, when a fault occurs, bearings and gears manifest repetitive transients in the time domain [14]. Thanks to the great efforts made by Antoni [15] and Antoni and Randall [16], the spectral kurtosis (SK) method was proposed to quantify the impulsiveness of repetitive transients, and in their subsequent work, a fast kurtogram method [17] was submitted for the detection of transient faults. Since then, SK has been

Received 7 May 2024; revised 15 August 2024; accepted 25 September 2024. Date of publication 14 October 2024; date of current version 25 October 2024. This work was supported in part by the National Natural Science Foundation of China under Grant 52375125 and Grant 52105117 and in part by the National Science and Technology Major Project under Grant J2019-IV-0018. The Associate Editor coordinating the review process was Dr. Marco Agustoni. *(Corresponding authors: Yu Sun; Laihao Yang.)*

Yingchun Li, Yu Sun, Xuefeng Chen, and Laihao Yang are with the School of Mechanical Engineering, Xi'an Jiaotong University, Xi'an 710049, China (e-mail: lyc3122301072@stu.xjtu.edu.cn; yu.sun@xjtu.edu.cn; yanglaihao@xjtu.edu.cn; chenxf@xjtu.edu.cn).

Zhiyuan Li is with China Railway Eryuan Engineering Group (CREEC) (Chongqing) Survey Design and Research Company Ltd., Chongqing 401120, China (e-mail: lizhiyuan24@ey.crec.cn).

Digital Object Identifier 10.1109/TIM.2024.3480226

extensively utilized in the CM and fault feature extraction of rotating machinery. Subsequently, additional sparse methods were investigated to quantify faulty impulses and used as HIs, such as smoothness index [18], negative entropy [19], and Gini index [20]. Wang et al. [21] consolidated these sparse methods into a generalized framework named the sum of the weighted normalized square envelope (SWNSE). Then, they proposed weight design methodologies based on domain knowledge and data-driven approaches for designing the new PHI. Based on SWNSE, Hou et al. [22] revealed the physical significance of the positive and negative optimization weights in the weighted normalized square spectrum (SWNFS). These weights enable differentiation between fundamental frequency components and fault-generated frequency components. Some scholars integrate signal processing methods with statistical indicators to formulate robust HIs. Miao et al. [23] performed singularity analysis employing the Lipschitz exponent function and developed a kurtosis-based HI to quantify the degradation process of gears. Antoni and Borghesani [24] presented a novel statistical method to design PHIs based on the principle of a maximum likelihood ratio, which can track cyclostationary or non-Gaussian symptoms independently. In addition, a pioneering framework for constructing optimal PHI is proposed [25], offering a significant advancement in the early detection of machine faults through a rigorous statistical approach. Due to the constructive nature of these metrics, they can recognize early failures in a timely manner. Although the aforementioned PHIs possess clear physical interpretations and are effective in extracting fault characteristics, they may not always capture monotonic degradation trends and necessitate expert knowledge for flexible usage.

In recent years, due to the advances in sensor technology, a large amount of sensed data can be used for HI construction, and VHI construction based on feature-level fusion and machine learning methods has become a hot research field in CM. For example, Guo et al. [26] proposed a recurrent neural network-based VHI by fusing multiple classic bearing fault features in the time domain, frequency domain, and time–frequency domain for assessing bearing conditions. Ocak et al. [27] used a hidden Markov model (HMM) to fuse multiple features derived from wavelet packet decomposition and calculated the probability of the HMM at the health stage as the VHI of the bearing, which will decrease significantly when the bearing approaches failure. Wang et al. [28] designed a high-order complex Comblet to extract signals associated with gear faults, acquiring acceleration error signals. Subsequently, an HMM was constructed to build an HI to assess the degradation of gear performance. These scholars conduct feature fusion by feature extraction on large data and uncover valuable information suitable for CM within the amalgamation of these features. Furthermore, additional researchers enhance monitoring outcomes by integrating diverse machine learning models. For example, Zhang et al. [29] proposed continuous HMM-based negative log-likelihood probability (CHMM-based LLP) to acquire a sensitive bearing degradation indicator that exhibits a significant trend. Aye et al. [30] presented an integrated approach that combines Gaussian mixture modeling (GMM) with kernel principal component analysis (KPCA) and exponentially weighted moving average (EWMA), resulting in a quantitative metric for acoustic emission (AE) referred to as the degradation assessment index (DAI). Due to the powerful data dimensionality reduction and feature extraction capabilities of PCA, it has a wide range of applications in feature-level fusion for CM. Dong and Luo [31] applied PCA to merge and reduce the dimensionality of multiple features from the time, frequency, and time–frequency domains. They then constructed and trained an optimized LS-SVM model using the extracted typical sensitive features to predict the bearing degradation process. Widodo and Yang [32] employed PCA for dimensionality reduction of time domain features, thereby shortening the RVM network training time. In addition, they constructed the VHI by calculating the deviation between the unknown states and healthy states. Some other PCA-related CM methods are provided in [33], [34], [35], [36], and [37]. However, the above PCA-related methods for CM are employed for feature extraction or as data preprocessing methods for specific network learning tasks. As far as we know, it lacks a PCA-based method for direct CM, which may provide interpretability and efficiency to the greatest extent.

B. Approach and Contributions

VHIs usually yield superior results compared to PHIs in general, but they often suffer from a lack of interpretability. For instance, understanding machine learning and AI model construction, along with their extracted features, is challenging, impeding the comprehensive explanation of VHI performance. The majority of current VHI construction models suffer from a deficiency in model transparency and interpretability. Therefore, some explainable applications of machine learning methods for building HIs in CM need to be studied. This article explores novel interpretable applications of PCA, identifying and elucidating the unique performance of the dimensionality reduction technique PCA within a specific process. In contrast to the feature-fusion and model-fusion approaches discussed in prior literature, this study demonstrates that it is possible to achieve CM, automatic threshold setting, and automatic fault feature extraction simultaneously by applying PCA downscaling to the degraded data spectra of rotating machinery.

The main contributions of this article are summarized as follows.

1) First, through PCA downscaling applied to the frequency domain of rotating machinery degradation data, it is theoretically illustrated that the physical significance of the spectral principal components (PCs) aligns with the VHI derived from data-level fusion. Consequently, the spectral PC itself can serve directly as an HI for CM.
2) The employment of the PC-based Fourier spectrum (PCBFS) serves to facilitate noise suppression, thereby enhancing the prominence of the information band. Furthermore, PCBFS-2 enables automated feature extraction, aiding in identifying defective and healthy frequency components, thereby enabling fast fault diagnosis.

3) This study leverages the traditional PCA method to reveal novel findings regarding its performance within a defined process. It investigates the intricate effects of these methods from various perspectives, offering a fresh perspective on the integration of data-driven modeling with machine learning techniques.

The rest of this article is organized as follows. Section II briefly presents the theoretical basis of the PCA. Afterward, it is theoretically illustrated that the proposed method can be used for CM and identification between fault signatures and healthy components. Simulated bearing degradation data were used to validate the proposed method in Section III. Experimental verifications using bearing and gear run-to-failure datasets are given in Section IV. Finally, conclusions are drawn in Section V.

II. Theoretical Investigations

In this section, the basic idea of the PCA is briefly introduced, and an explicit expression of an optimal projection direction is then given. Afterward, it is illustrated that the PC vectors of the degradation data spectrum can be directly used for CM and provide the theoretical basis. Simultaneously, with the help of the mathematical relationship between PCs and experience, it is concluded that the second PC-based Fourier spectrum (PCBFS-2) can discriminate the frequency components. The technical processes of the spectra PCA downscaling for CM and automatic fault feature extraction are summarized in Fig. 2.

A. Technical Preliminaries: PCA

PCA is a widely used dimensionality reduction technique that transforms a set of correlated variables into a set of uncorrelated variables, known as PCs. The primary objective of PCA is to identify the directions (PCs) that maximize the variance in the data.

To ensure the accuracy of the PCA, the data matrix $\boldsymbol{X}$ must first be centered. This involves subtracting the mean of each feature from the corresponding feature values across all observations

$$\boldsymbol{X_c} = \boldsymbol{X} - \mu \tag{1}$$

where μ is the mean vector of the data, calculated as $\mu = (1/n)\sum_{i=1}^{n} x_i$, and x_i represents the ith observation in the dataset. With the centered data, the covariance matrix $\boldsymbol{C}$ is computed as

$$\boldsymbol{C} = \frac{1}{n-1}\boldsymbol{X}_c\boldsymbol{X}_c^T \tag{2}$$

where C represents the variances and covariances between the different features. The PCs are found by solving the eigenvalue problem for the covariance matrix $\boldsymbol{C}$

$$\boldsymbol{C}\boldsymbol{\omega}_i = \lambda_i\boldsymbol{\omega}_i \tag{3}$$

where λ_i are the eigenvalues and $\boldsymbol{\omega}_i$ are the corresponding eigenvectors. The eigenvectors $\boldsymbol{\omega}_i$ represent the directions of the PCs, and the eigenvalues λ_i indicate the amount of variance each component explains.

The centered data $\boldsymbol{X}_c$ are then projected onto the PCs to obtain the PC scores

$$\hat{\boldsymbol{x}}_{\boldsymbol{i}} = \boldsymbol{\omega}_i^T\boldsymbol{X}_c. \tag{4}$$

This results in a set of PCs $\hat{\boldsymbol{X}} = [\hat{\boldsymbol{x}}_1, \hat{\boldsymbol{x}}_2, \ldots, \hat{\boldsymbol{x}}_k]$. These components are uncorrelated and are ordered by the variance they explain, enabling effective dimensionality reduction while retaining the most significant patterns in the data.

B. Physical Interpretation of Spectral PC Vector

In this section, we apply the PCA downscaling method for CM of rotating machinery. Let a machine run-to-failure dataset be $\boldsymbol{V} = [\boldsymbol{v}_1, \boldsymbol{v}_2, \cdots \boldsymbol{v}_n]$, where $\boldsymbol{v}_i \in R^{d\times 1}$ is the data sample taken at fixed intervals, typically stored in a data file with a length of d. n represents the total data files collected from the machine life cycle. Hence, a run-to-failure dataset $\boldsymbol{V} \in R^{d\times n}$ can be expressed as follows:

$$\boldsymbol{V} = [\boldsymbol{v}_1\boldsymbol{v}_2\ \cdots \boldsymbol{v}_n] = \begin{bmatrix} v_{1,1} & v_{2,1} & \cdots & v_{n,1} \\ v_{1,2} & v_{2,2} & \cdots & v_{n,2} \\ \vdots & \vdots & \vdots & \vdots \\ v_{1,d} & v_{2,d} & \cdots & v_{n,d} \end{bmatrix} \tag{5}$$

where v_{ij} is the jth sample point in the ith file number. The frequency domain contains rich feature information. Based on the fast Fourier transform (FFT) technique, we can convert the data matrix from the time domain to the frequency domain

$$\boldsymbol{F} = \mathrm{FFT}([\boldsymbol{v}_1\boldsymbol{v}_2\cdots\boldsymbol{v}_n]) = \begin{bmatrix} f_{1,1} & f_{2,1} & \cdots & f_{n,1} \\ f_{1,2} & f_{2,2} & \cdots & f_{n,2} \\ \vdots & \vdots & \vdots & \vdots \\ f_{1,k} & f_{2,k} & \cdots & f_{n,k} \end{bmatrix} \tag{6}$$

where $\mathrm{FFT}(\cdot)$ is the computational process that obtains the amplitude values of the spectral lines of the signal and $f_{n,k}$ denotes the amplitude value of the kth spectral line of the time-domain signal $\boldsymbol{v_n}$. By employing PCA dimensionality reduction on the frequency domain data matrices and solving the eigenvalue problem of $\boldsymbol{F}^T\boldsymbol{F}$, we can obtain the transformation matrix $\boldsymbol{P}$, $\boldsymbol{P} = [\boldsymbol{\omega}_1, \boldsymbol{\omega}_2, \ldots, \boldsymbol{\omega}_n]$, which can transform the original data matrix into a lower dimensional space. Each column of the transformation matrix is a feature vector arranged in descending order of the eigenvalues, also known as the PC vectors. In this study, we call them spectral PCs (SPCs). Then, we can select one of these SPCs to reconstruct the spectrum matrix and obtain the ith spectral PC-based Fourier spectrum (PCBFS-i). The mathematical form is $\hat{\boldsymbol{F}}_i = \boldsymbol{F} \times \boldsymbol{\omega}_i$ and $\hat{\boldsymbol{F}}_i \in R^{k\times 1}$. As noise-related components are typically associated with the coordinate direction of smaller eigenvalues [38], [39], using feature vectors corresponding to larger eigenvalues to represent the frequency data can achieve the effect of spectrum noise reduction and highlighting feature frequencies.

Thus, we can use the obtained new spectral data (PCBFS-i) as weights to the original spectrum, thereby constructing an

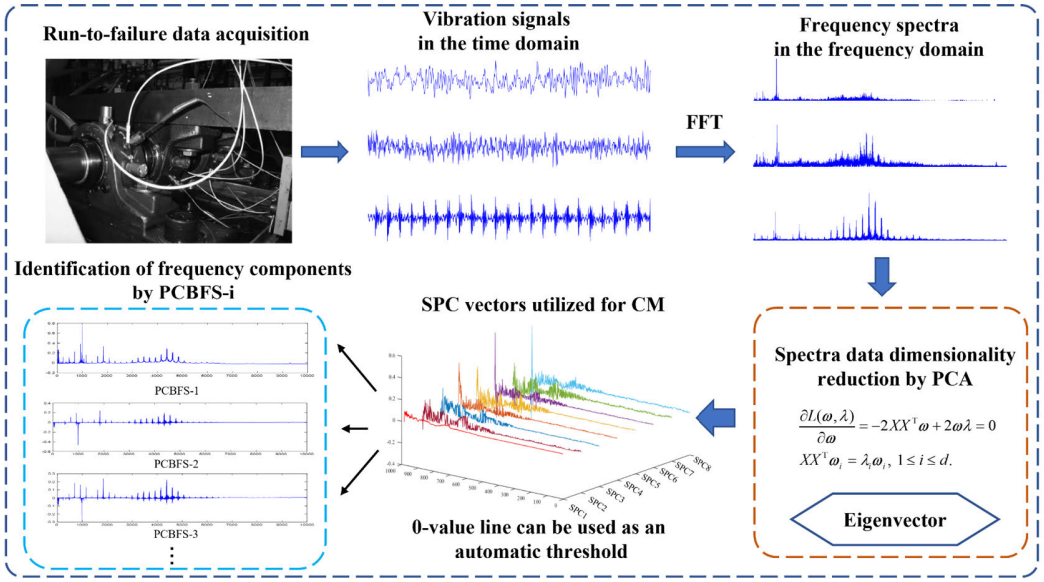

Fig. 2. Flowchart of the spectra PCA downscaling for CM and automatic fault feature extraction.

HI through the data-level fusion of spectrum amplitudes. The HI is designed as follows:

$$\mathrm{HI} \in R^{n\times 1} = \boldsymbol{F}^T \times \mathrm{weight} = \begin{bmatrix} f_{1,1} & f_{1,2} & \cdots & f_{1,k} \\ f_{2,1} & f_{2,2} & \cdots & f_{2,k} \\ \vdots & \vdots & \vdots & \vdots \\ f_{n,1} & f_{n,2} & \cdots & f_{n,k} \end{bmatrix} \times \begin{bmatrix} \hat{f}_{i,1} \\ \hat{f}_{i,2} \\ \vdots \\ \hat{f}_{i,k} \end{bmatrix} \tag{7}$$

where i is the serial number of the spectral PC, $\hat{\boldsymbol{f}}_i (1 \le i \le n)$ is the projection coordinate of the spectrum in the SPC i th direction, and $\hat{f}_{i,k}$ is the amplitude of the k Hz spectral line in $\hat{\boldsymbol{f}}_i$. Although the constructed HI is part of the VHI, it is not simply a fusion of models and data but has some physical significance. The rationale for building this HI is to use the appropriate PCBFS-i to reduce spectral noise and to highlight the impact of information bands (health-related information and fault frequencies and their harmonics). In other words, it is conceivable that PCBFS-i is "filtered" to enhance fault-related frequencies and suppress noise. Through experiments, we have observed that the degradation trend quantified by the constructed HI is consistent with the corresponding PC trend, as shown in Fig. 3. From (8), we can infer that the constructed HI is a multiple of the PC, and this multiple exactly equals the eigenvalues corresponding to the PC. This also indicates that the SPC has the same physical meaning and role as the constructed HI. Then, in practical use, instead of constructing the HI, the SPCs can be directly used for CM through the frequency domain dimensionality reduction

$$\mathrm{HI} = \boldsymbol{F}^T\hat{\boldsymbol{F}} = \boldsymbol{F}^T(\boldsymbol{F}\boldsymbol{\omega}_i) = \left(\boldsymbol{F}^T\boldsymbol{F}\right)\boldsymbol{\omega}_i = \lambda\boldsymbol{\omega}_i. \tag{8}$$

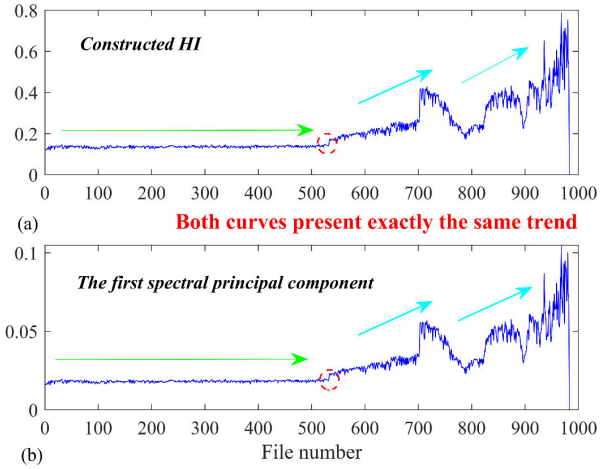

Fig. 3. Monitoring curve of IMS data quantified by (a) constructed HI and (b) first spectral PC.

C. PCBFS-2 for Automatic Frequency Components Recognition

Since the higher order PCs have less information content and fluctuate more, which is not conducive to analyzing the changes in the state of the equipment, only the first two PC vectors are taken for analysis in this study. PCBFS-1 and PCBFS-2 are given by the following equation:

$$\hat{\boldsymbol{F}}_{1,2} = \boldsymbol{F} * \boldsymbol{P}_{1,2} = \begin{bmatrix} f_{1,1} & f_{2,1} & \cdots & f_{n,1} \\ f_{1,2} & f_{2,2} & \cdots & f_{n,2} \\ \vdots & \vdots & \vdots & \vdots \\ f_{1,k} & f_{2,k} & \cdots & f_{n,k} \end{bmatrix} \times \begin{bmatrix} \omega_{1,1} & \omega_{2,1} \\ \omega_{1,2} & \omega_{2,2} \\ \vdots & \vdots \\ \omega_{1,n} & \omega_{2,n} \end{bmatrix} = \begin{bmatrix} \hat{f}_{1,1} & \hat{f}_{2,1} \\ \hat{f}_{1,2} & \hat{f}_{2,2} \\ \vdots & \vdots \\ \hat{f}_{1,k} & \hat{f}_{2,k} \end{bmatrix} \tag{9}$$

where $\boldsymbol{P}_{1,2} = [\boldsymbol{\omega}_1, \boldsymbol{\omega}_2]$. From (9), it can be observed that the PCBFS is a linear combination of each spectral line using the SPC vector, denoted as ω. It can be expressed as follows:

$$\hat{f}_{1,h} = \sum_{i=1}^{n} f_{i,h} \times \omega_{1,i},\ \hat{f}_{2,h} = \sum_{i=1}^{n} f_{i,h} \times \omega_{2,i} \tag{10}$$

where $\hat{f}_{1,h}$ and $\hat{f}_{2,h}$ represent the linear combination of the spectral lines in the spectrums of n samples with frequency h Hz under the first two SPCs.

As shown in Fig. 4, the fundamental frequency's amplitude, which is unrelated to the fault, such as the shaft rotating frequency, does not change much during the degradation process. However, the change in the amplitude of the fault-related frequency reflects the degradation process of the bearing, although it is not apparent. Thus, according to this proposition, if h Hz is the fundamental frequency and stays as f_h through the life cycle, (10) can be approximately reformulated as

$$\hat{f}_{1,h} \approx f_h \sum_{i=1}^{n} \omega_{1,i},\ \ \hat{f}_{2,h} \approx f_h \sum_{i=1}^{n} \omega_{2,i}. \tag{11}$$

The first spectral PC contains the most comprehensive signal information due to its largest eigenvalues and is the best suited to restore the composition of the signal. Since the spectral components are nonnegative in amplitude, $\boldsymbol{f}_h > 0$, the signal projection on the first PC should also be nonnegative, namely, $\hat{f}_{1,h} > 0$. As the covariance matrix is symmetric, its eigenvectors are orthogonal to each other, $\sum_{i=1}^{n} \omega_{1,i} \times \omega_{2,i} = 0$. Since SPC 1 is all positive, there must be negative values in SPC 2. Also, both PCs indicate the degradation trend of the faults, which means that they consist of a period of a smooth health phase and a numerical rising fault phase. The trend of the second PC is to start with a negative number and start to become larger with the occurrence of faults. Due to the scarcity of abnormal occurrences in the time dimension, the majority of SPC 2 values are negative, leading to an overall negative sum of SPC 2. Our data experiments prove that even if the failure occurs, the value of the second PC increases to a positive number, and the sum of the values of SPC 2 is still negative, namely, $\sum_{i=1}^{n} \omega_{2,i} < 0$. Then, $\hat{f}_{2,h} = \boldsymbol{f}_h \sum_{i=1}^{n} \omega_{2,i} < 0$; therefore, the amplitude of the fundamental frequency under the direction of SPC 2 tends to become negative. The amplitude of the fundamental frequencies expressed under the direction of the two PCs has the relationship as shown in (12). Simultaneously, the value of SPC 2 exhibits an upward trajectory with the degradation of bearings or gears, increasing rapidly to a positive number following the onset of early faults. At this juncture, the 0 value axis, employed as a segmentation threshold, can serve as an alarm threshold to identify the occurrence of faults. At this stage, the fault has progressed to a certain extent and is likely to impact the normal operation of the machine in the subsequent evolution process. Consequently, a threshold is established to trigger an alarm, notifying the operator to decide whether to initiate shutdown for maintenance, among other considerations

$$\frac{\hat{f}_{1,h}}{\hat{f}_{2,h}} \approx \frac{f_h \sum_{i=1}^{n} \omega_{1,i}}{f_h \sum_{i=1}^{n} \omega_{2,i}} = \frac{\sum_{i=1}^{n} \omega_{1,i}}{\sum_{i=1}^{n} \omega_{2,i}}. \tag{12}$$

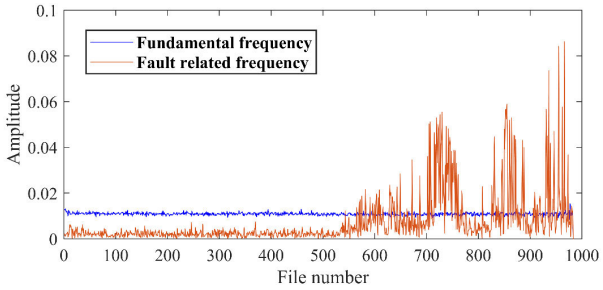

Fig. 4. Fundamental frequency (50 Hz) amplitudes and fault-related frequencies (4388 Hz) amplitudes in all sample spectra.

The frequency associated with faults exhibits a variation pattern consistent with the machine degradation process. In Fig. 4, the amplitude variation pattern of the 4388-Hz spectral line for bearing 1 displays more fluctuations compared to SPC 1 in Fig. 3(b), but the overall trend remains consistent. Unlike the fundamental frequency, which is solely linked to the sum of SPC values, the behavior of the fault-related frequency in PCBFS-2, namely, $\hat{f}_{2,f} = \sum_{i=1}^{n} f_{i,f} \times \omega_{2,i}$, is influenced not only by the values of SPC but also by the fault evolution process. The fault frequency $f_{i,f}$ always maintains a positive value, $\omega_{2,i}$ in SPC 2 transitions from negative to positive after the fault occurrence, and both exhibit an overall upward trend. This amplification of the positive value in SPC 2 ensures that the final summation result $\hat{f}_{2,f}$ remains positive. This means that the amplitude of the fault frequency remains positive in PCBFS-2. Consequently, PCBFS-2 can distinguish between the fundamental and fault-related frequencies. This accomplishes a comparable outcome as seen in [22], yet our method eliminates the necessity for human feature selection for model training.

In this section, we have indicated that the SPC is mathematically equivalent to an HI designed based on spectral weighting, elucidating why SPC can be directly utilized as a monitoring metric. In the domain of rotating machinery PHM, prior knowledge is often reflected in the frequency components, and the study of these frequency components aids in our assessment of the method's interpretability. Subsequently, we further analyzed the spectral component variations in the direction of the PCs, namely, the study of PCBFS. It is noted that different PCBFSs serve the purpose of observing frequency changes and identifying frequency components and the learned frequency components are interpretable and consistent with prior knowledge. These points will be validated through a simulation experiment and two experiments on rotating machinery components.

III. Performance Investigation via Simulations

In this section, a set of bearing run-to-failure data is simulated to verify the proposed method, including the evaluation of SPC's ability to represent the degradation process and PCBFS-i's capability to distinguish frequency components. Following the previous works [40], [41], the vibration signal is expressed as

$$v(t) = h(t) + r(t) + G \tag{13}$$

TABLE I
PARAMETER SETTINGS FOR HARMONIC SIGNALS AND REPETITIVE TRANSIENTS

Parameter	Value	Parameter	Value	Parameter	Value
h_1	0.8	h_2	1.2	h_3	0.5
f_1	30	f_2	50	f_3	75
φ_1	$\pi/3$	φ_2	$\pi/6$	φ_3	$\pi/4$
T	1/59	ζ	300	f_r	2000

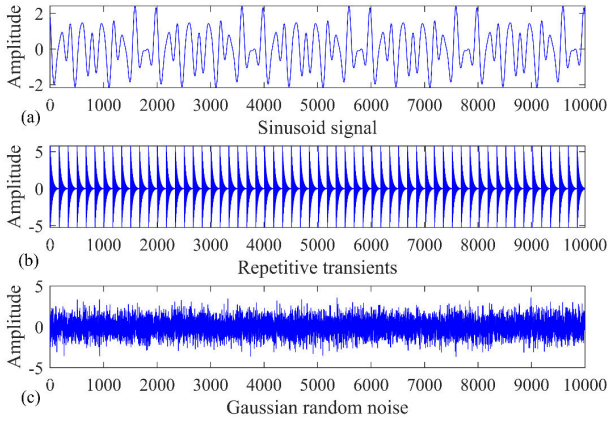

Fig. 5. Simulated signals. (a) Harmonic signal. (b) Repetitive transients in file 900. (c) Gaussian random noise.

where $h(t)$ are the harmonic signals, $r(t)$ is the repetitive transient associated with the fault, and G is the Gaussian random noise. The harmonic signal comprises several individual harmonic signals with different amplitudes and frequencies that exist throughout the bearing's life cycle

$$h(t) = \sum_m H_m \cos(2\pi f_m t + \varphi_m) \tag{14}$$

$r(t)$ represents the repetitive transient caused by machine failure. A_n is the amplitude of the nth transient signal and T corresponds to its occurrence time. The damping ratio of the repetitive transient is denoted as ζ, and f_r is the resonance frequency

$$r(t) = \sum_n A_n \delta(t - T). \tag{15}$$

Equation (15) indicates the periodic impulse signal $r(t)$ with a period T caused by the outer race fault of the bearing, and the modeling of a single impulse signal within the periodic signal is defined as

$$\delta(t) = e^{-\zeta t} \sin(2\pi f_r t). \tag{16}$$

The signal G is a Gaussian random noise signal following a standard normal distribution. The parameter settings for harmonic signals and repetitive transients are outlined in Table I. The obtained harmonic signal and Gaussian random noise signal are shown in Fig. 5(a) and (c), respectively.

To simulate the signals of the bearing degradation process, assuming that 1000 data files are collected, each with a sampling frequency of 10 kHz and a sampling time of 1 s, resulting in 10 000 data points per file. The bearing's degradation process is simulated by varying the value of A_n in the repetitive transient signal. For this study, the fault occurrence point is set at data file 800. The amplitude of the simulated transient signal varies from 0 to 5 in increments of 0.025, ranging from data file 800 to 1000. To achieve a more realistic simulation of the bearing degradation trend, the obtained repetitive transient amplitude sequence is squared. Thus, we can get the simulated bearing degradation signal $\boldsymbol{V} \in \boldsymbol{R}^{10000\times1000}$. The overview of the Fourier spectra of the simulated signal is depicted in Fig. 6. It can be observed that the resonance band around 2000 Hz starts to appear after file 800, and its amplitude increases with the degradation process. In contrast, the three fundamental frequency components, 30, 50, and 75 Hz, persist throughout the entire cycle.

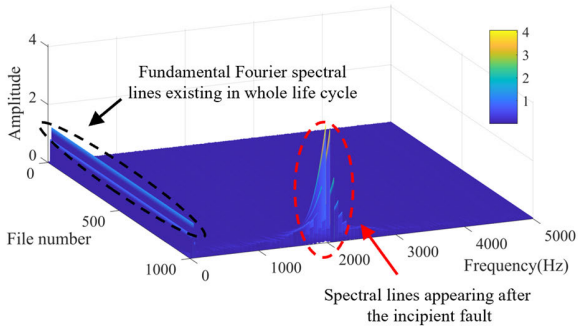

Fig. 6. Overview of the Fourier spectra of the simulated signal.

After obtaining the simulated bearing degradation signal, we perform FFT on the signal and solve the eigenvalue problem of the data covariance matrix in the frequency domain data matrix, namely, $\boldsymbol{F}^T\boldsymbol{F}$. Subsequently, we can obtain the SPC vectors and the corresponding PCBFS, as shown in Figs. 7 and 8. As previously analyzed, both spectral PC vectors can represent the bearing degradation process, and SPC 2 starts from a negative value and increases when the fault occurs. The 0-value line in SPC 2 serves as an automatically set threshold, and an alarm is generated when SPC 2 exceeds this threshold. The plots in Fig. 7(b) show that the PCBFS-1 is dominated by three harmonic spectral lines and the resonance frequency bands. In PCBFS-2 of the simulated bearing signal, the amplitudes of the fundamental frequency become negative, while the spectral lines in the resonance frequency bands stay positive. To verify (12), the sum of the two spectral PCs is calculated as 61.3646 and -35.1338, and the ratio is -1.7466. Taking the amplitude of the 75-Hz spectral line as an example, the ratio of the two amplitudes in PCBFS-1 and PCBFS-2 is $30.1976/(-17.4678) = -1.7288$. The error between the ratio of the sum of the two PCs is only 1%. Thus, the application of the proposed method in CM and feature extraction has been verified separately.

IV. VERIFICATION BY USING BEARING AND GEAR RUN-TO-FAILURE DATASETS

Bearings and gears are widely used rotating machinery in engineering, and monitoring their condition is crucial to ensuring safe machine operation and timely detection of faults,

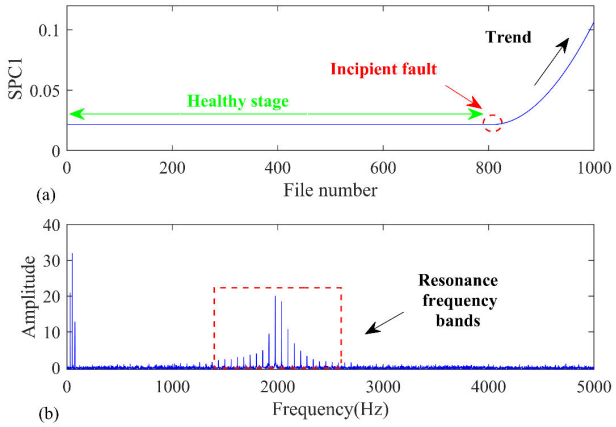

Fig. 7. Simulated bearing run-to-failure data case. (a) SPC1 vector. (b) PCBFS-1.

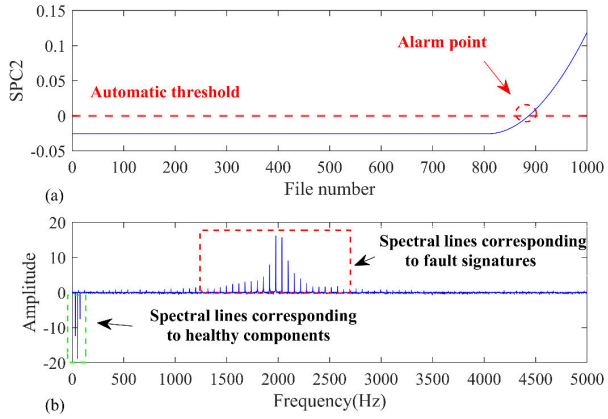

Fig. 8. Simulated bearing run-to-failure data case. (a) SPC2 vector. (b) PCBFS-2.

thereby reducing economic losses. In this section, bearing and gear run-to-failure datasets are employed to validate the effectiveness of the proposed method.

A. First Case Study: Verification by Bearing Run-to-Failure Datasets

The bearing run-to-failure dataset [42] was provided by the Intelligent Maintenance Systems Center at the University of Cincinnati, and the test rig is shown in Fig. 9. Vibration signals were collected from four bearings at a shaft speed of 2000 RPM with a sampling frequency of 20 kHz. The experiment resulted in three datasets, including vibration signals of bearings with outer race faults, inner race faults, and rolling element faults. In the experiment, bearing 1 experienced an outer race fault with a fault frequency of 236 Hz. A total of 984 vibration signal data files were collected during the life cycle, with each data file containing 20 480 points.

First, in order to have a preliminary understanding of bearing1's overall degradation trend for performance degradation assessment (PDA), four popular sparse measures are calculated to quantify this dataset by the following equations:

$$\text{Kurtosis} = \frac{\sum_{n=1}^{N} \text{SE}^2[n]/N}{\left(\sum_{n=1}^{N} \text{SE}^2[n]/N\right)^2} \tag{17}$$

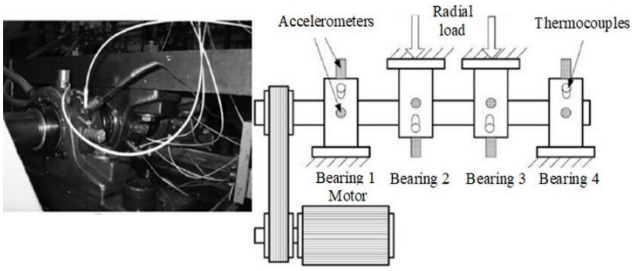

Fig. 9. Test rig of IMS bearing run-to-failure datasets.

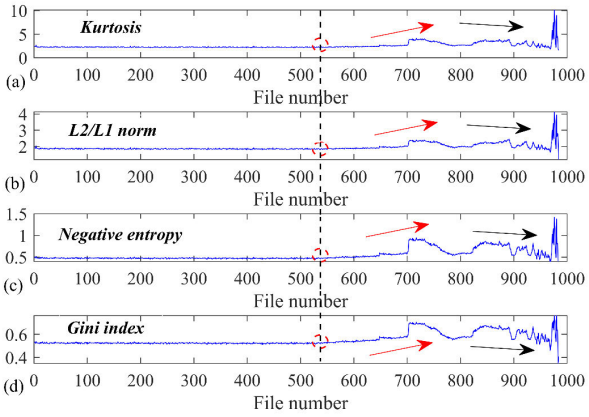

Fig. 10. Four popular sparse measures for PDA of bearing 1. (a) Kurtosis. (b) L2/L1 norm. (c) Negative entropy. (d) Gini index.

$$\text{L2/L1 norm} = \sqrt{N}\frac{\sqrt{\sum_{n=1}^{N} \text{SE}^2[n]}}{\sum_{n=1}^{N} \text{SE}[n]} \tag{18}$$

$$\text{NE} = \left\langle \frac{(\text{SE}[n])}{\langle \text{SE}[n] \rangle} \ln\left(\frac{(\text{SE}[n])}{\langle \text{SE}[n] \rangle}\right) \right\rangle \tag{19}$$

$$\text{GI} = 1 - 2\sum_{n=1}^{N} \frac{\text{SE}_{\text{order}}[n]}{\sum_{n=1}^{N} \text{SE}[n]} \left(\frac{N - n + 1/2}{N}\right) \tag{20}$$

where $\text{SE}[n]$ is the squared envelope of $x[n]$, $\langle \cdot \rangle$ is an arithmetic average operator, and SE_{order} is the ordered $\text{SE}[n]$ from the smallest to the largest. Taking into account the "self-healing" nature of damage [43], the state of bearing 1 undergoes multiple changes, thereby introducing additional complexity to the monitoring process. The quantification results by the four sparse methods are shown in Fig. 10. These four indicators are not able to clearly detect the incipient fault at file number 534; meanwhile, they also do not show a clear monotonic degradation trend.

In addition to the time-domain degradation characteristics of bearing 1 obtained by the four sparse methods, the frequency-domain characteristics of bearing 1 are given in Figs. 11 and 12. Fig. 11 represents the frequency spectrum of the healthy and faulty states, and Fig. 12 shows an overview of the Fourier spectra of bearing 1. It can be observed that the informative bands, indicated by the blue dashed circle in Fig. 11, only start to appear after the occurrence of the incipient fault, while some health-related spectral lines, indicated by the red dashed circle (e.g., some spectral lines around 985 Hz), stay throughout the whole cycle. However,

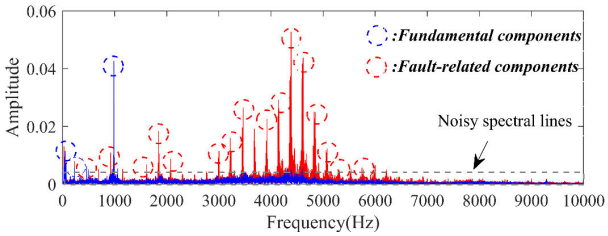

Fig. 11. Comparison of globally normal (blue solid lines) and abnormal spectral lines (red solid lines) of bearing 1.

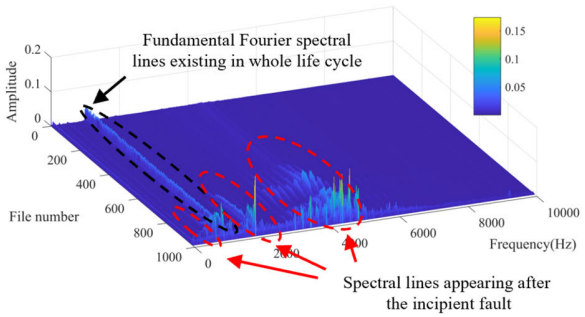

Fig. 12. Overview of the Fourier spectra of the bearing 1.

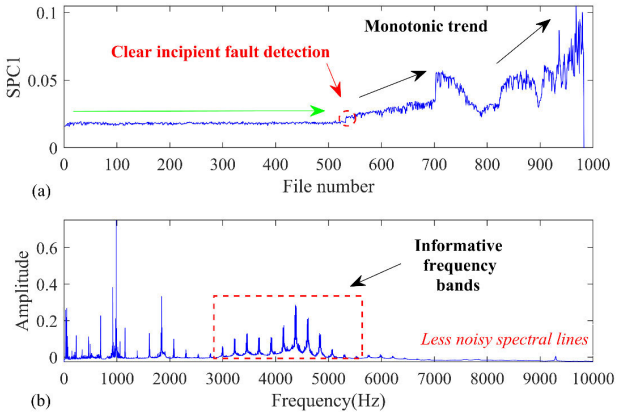

Fig. 13. IMS bearing case. (a) SPC1 vector. (b) PCBFS-1.

only some prominent spectral lines can be easily distinguished by human observation.

Afterward, the proposed method was employed. In practical applications, to ensure that the direct current (dc) component of the signal does not affect the judgment of the PC direction in the SPCA method, the mean-centering preprocessing method is applied to the signals to remove the dc component. The signal with the dc component removed is then analyzed by SPCA. SPC 1 and PCBFS-1, which are obtained by dimensionality reduction and spectrum reconfiguration of the frequency spectrum of 984 data files, are shown in Fig. 13. It can be observed that SPC 1 vector can present the degradation process of bearing1, and there is a clear incipient fault detection at file 534. Compared to the four sparse measures, SPC 1 also exhibits good monotonicity in the degradation trend, which is conducive to the prediction of the RUL at a later stage. In Fig. 13(b), noisy spectral lines are well suppressed, while

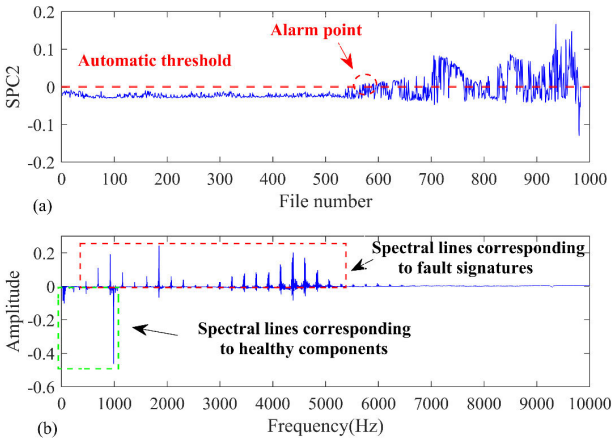

Fig. 14. IMS bearing case. (a) SPC2 vector. (b) PCBFS-2.

informative frequency bands, which lie in the frequency range of [3000, 5000] Hz, are highlighted in the PCBFS-1.

SPC 2 and PCBFS-2 of bearing 1 are plotted in Fig. 14. As the previous analysis of the variation pattern of SPC in Section II, the SPC 2 vector follows a pattern of increasing from negative values and gradually increasing to positive values with the appearance of failure characteristics while quantifying the bearing degradation process. The 0-value line in SPC 2 can be used as an automatically set threshold, and it can be seen that SPC 2 exceeds the threshold shortly after the fault occurs, realizing the alarm function. Due to the inconspicuous frequency of the fault components during the early fault period and the fluctuations in the SPC2 monitoring curve, the threshold in SPC2 exhibits a certain degree of latency in identifying early faults. Therefore, in practical applications, it is necessary to consider the degradation trends of both SPC1 and SPC2, along with the automatically set thresholds, to comprehensively indicate the degree of fault development.

Upon reaching a state of severe failure in the bearing, concomitant with the conclusion of the experiment, the sum of the two spectral PCs is calculated as 27.7355 and -9.682. The experimental outcome validates the assertion that the sum of SPC 2 values is indeed negative, in accordance with the stated observation. Meanwhile, the health-related spectral lines, indicated by the red dashed circles in Fig. 11, turn to negative values in PCBFS-2 in Fig. 14(b). Most notably, the spectral analysis reveals a prominent fundamental spectral line at 986 Hz, characterized by an amplitude of 0.7507 in PCBFS-1 and -0.4635 in PCBFS-2. Contrarily, the resonance frequency band of [3000, 5000] Hz, stimulated by the outer ring fault, consistently exhibits positive values. Moreover, the frequency interval between the peaks, indicated by the blue dashed circles in Fig. 11, within this resonance frequency band is approximately equal to the fault frequency of the outer ring, specifically 236 Hz for bearing 1.

To further illustrate the superior suitability of the proposed spectral PCA method for prognostic analysis compared to the commonly used sparse methods, we employ widely recognized metrics, including monotonicity, trendability, and robustness to SPC 1 and four sparse methods. The calculation methods

TABLE II
COMPARISONS OF HI FOR PROGNOSTIC ANALYSIS OF BEARING 1 IN MONOTONICITY, TRENDABILITY, AND ROBUSTNESS (M, T, AND R FOR SHORT)

Name	Kurtosis	L2/L1 norm	Negative entropy	Gini index	SPC1
M	0.005	0.009	0.068	0.101	0.274
T	0.549	0.545	0.639	0.676	0.789
R	0.996	0.998	0.997	0.999	0.993
Sum	1.550	1.552	1.704	1.776	2.056

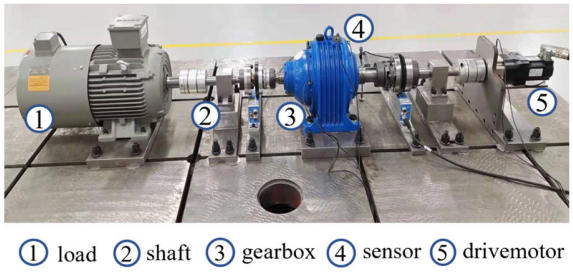

Fig. 15. Test rig of the gear run-to-failure datasets.

for these metrics can be found in [10]. From the results in Table II, it can be concluded that the proposed SPC 1 demonstrates superior performance compared to the four commonly used sparse methods. From the perspective of computational efficiency, under the same hardware and computational environment, the computation time for SPC is 0.8758 s, while the computation times for the four sparse methods are 0.4064, 0.4941, 0.4952, and 70.086 s. Although the proposed method may be outperformed by some sparse indicators in terms of program running time, its operational efficiency is still commendable. Compared to advanced artificial intelligence models, the proposed method has a distinct advantage in computational cost, as most AI methods require iterative training to achieve the optimal model. Although AI-driven methods may yield better numerical results, the proposed method offers superior interpretability and generalization performance. Moreover, the SPCA method can simultaneously achieve CM, threshold setting, and frequency component identification, which is akin to killing three birds with one stone. Based on the above observations, it can be concluded that the proposed method is experimentally verified.

B. Second Case Study: Verification by Gear Run-to-Failure Datasets

To further validate the proposed method, a self-collected gear run-to-failure dataset is investigated. The structure of the planetary gearbox test rig is shown in Fig. 15. Vibration signals were obtained using an accelerometer placed on the housing of the experimental gearbox, and the sampling frequency was set as 10 000 Hz. Data were collected for 2 min every 10 min, continuously for 24 h. The experiment stopped when the amplitude of the collected samples exceeded a certain level. At the end of the experiment, both the Sun gear and planetary gear experienced wear failure, and 694 data files were saved and collected.

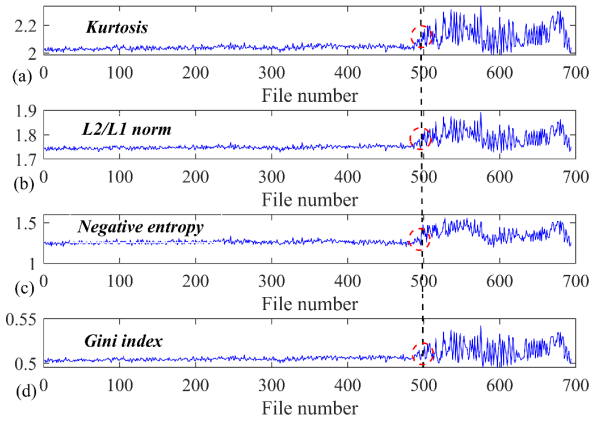

Fig. 16. Four popular sparse measures for PDA of the fault gear. (a) Kurtosis. (b) L2/L1 norm. (c) Negative entropy. (d) Gini index.

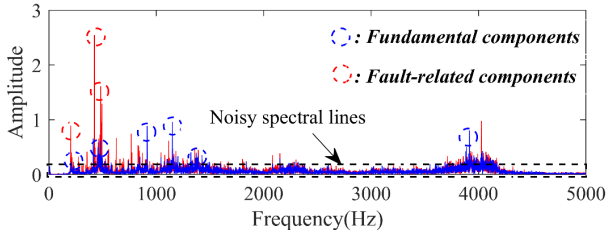

Fig. 17. Spectrum of health signals at file 10 (blue solid lines) and fault signals of the gear at file 500 (red solid lines).

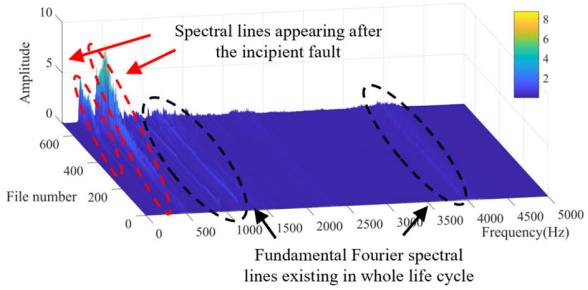

Fig. 18. Overview of the Fourier spectra of the gear.

Similarly, four popular sparse methods are used to quantify the degradation process for this run-to-failure gear dataset. As shown in Fig. 16, all four HIs detect the incipient fault around file 500 and start to fluctuate sharply, but none show the gear's monotonic degradation process. The frequency-domain characteristics of the gear are given in Figs. 17 and 18. Fig. 17 illustrates the spectra of healthy and faulty states, and an overview of the Fourier spectra of the gear is shown in Fig. 18. Fault-related frequency components, indicated by blue dashed circles in Fig. 17, appear around file 500. In addition, some fundamental frequencies, such as the meshing frequency and its harmonics and some unknown frequency components around 4000 Hz, which may be attributed to a high-frequency weak excitation signal arising from issues in the experimental environment, such as the installation of the experimental bench or weak signals generated by the surrounding test bench, keep staying throughout the entire experimental cycle.

TABLE III
COMPARISONS OF HI FOR PROGNOSTIC ANALYSIS OF THE GEAR IN MONOTONICITY, TRENDABILITY, AND ROBUSTNESS (M, T, AND R FOR SHORT)

Name	Kurtosis	L2/L1 norm	Negative entropy	Gini index	SPC1
M	0.007	0.039	0.027	0.001	0.732
T	0.603	0.616	0.597	0.580	0.873
R	0.999	0.999	0.998	0.999	0.994
Sum	1.609	1.654	1.622	1.580	2.599

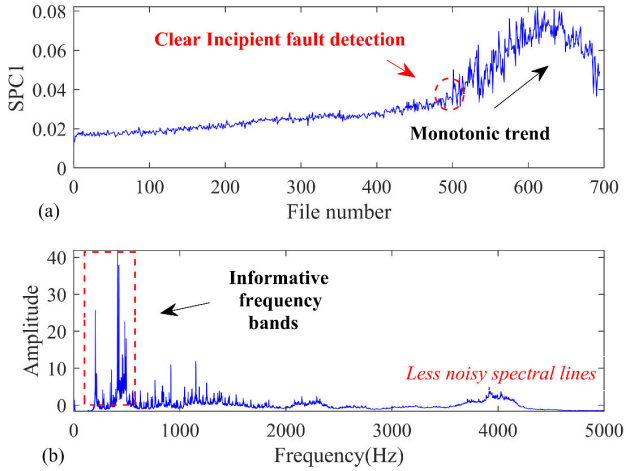

Fig. 19. Gear run-to-failure case. (a) SPC1 vector. (b) PCBFS-1.

By performing PCA dimensionality reduction on the spectral data matrix of this set of degraded gear data, the spectral PCs are obtained. As shown in Fig. 19, it can be observed that around file 500, SPC 1 starts to rise dramatically and shows a monotonous degradation trend. Meanwhile, compared to the spectrum in Fig. 17, there are less noisy spectral lines and more prominent informative frequency components in PCBFS-1. The comparison results of the degraded gear between the proposed SPC 1 and four popular sparse measures in monotonicity, trendability, and robustness are summarized in Table III. The measurement results affirm that the proposed SPC 1 exhibits superior performance for prognostic analysis. The running times for the proposed method and the four sparse methods are 0.4537, 0.2764, 0.464, 0.6231, and 47.449 s. The SPCA method still maintains commendable operational efficiency. Overall, the proposed method remains a robust and comprehensive approach.

To enable automatic threshold setting and automatically distinguish different frequency components, SPC 2 and PCBFS-2 of the gear are plotted in Fig. 20. The trend of SPC 2 is consistent with the previous analysis. Simultaneously, the thresholds are set automatically, and the alarm point appears after the incipient fault. Similar to IMS bearing 1, SPC2 has shown a certain degree of latency in indicating the early stages of gear faults. By combining the degradation curve of SPC1, it can be observed that the early fault occurred around file 500. In the event of gear failure, the amplitude of SPC 2 experiences an increase, manifesting as a positive

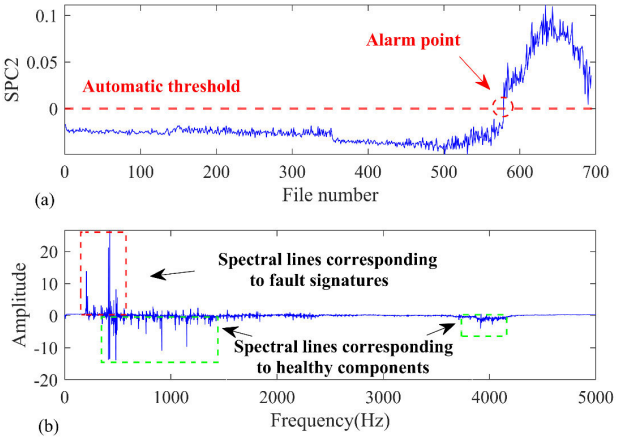

Fig. 20. Gear run-to-failure case. (a) SPC2 vector. (b) PCBFS-2.

number. However, it is noteworthy that the sum of SPC 2 values is calculated as −2.3884, indicating that it remains a negative value even during gear failure. For phenomena in the frequency domain, As shown in Fig. 20(b), the fundamental frequency and some frequency components present throughout the test cycle become negative in PCBFS-2. The most conspicuous observation is the amplitude transition of the 915-Hz spectral line, shifting from 11.0367 in PCBFS-1 to −10.9179 in PCBFS-2, along with the amplitude alteration of the 1150-Hz spectral line, transitioning from 11.8684 in PCBFS-1 to −9.74596 in PCBFS-2. Nevertheless, despite the increase in amplitudes associated with the meshing frequency (234 Hz) and double meshing frequency (468 Hz) due to gear wear, their amplitudes consistently remain positive in PCBFS-2.

Therefore, the proposed method can not only identify the informative frequency bands but also differentiate the healthy and faulty frequency components in PCBFS-2, a task that cannot be achieved by traditional sparsity-based methods [15].

V. CONCLUSION

This article explores the application of frequency-domain PCA dimensionality reduction for CM and frequency component identification. It proposes that the physical significance of the PCs obtained by spectral downscaling degraded data can be used as HIs for CM. The PCBFS can not only suppress noisy spectral lines and highlight the informative bands but also enable the automatic distinction between fundamental and fault-related frequencies through projections on different PCs. Subsequently, simulations and two degradation experimental studies are conducted to validate the propositions.

The innovations of this article lie in providing a new perspective to understand the significance of PCs in the frequency domain by constructing an HI through the data-level fusion of frequency amplitudes. Exploring the detailed effects of the SPCA method from various perspectives aims to serve as an example for the innovative application of other traditional methods. In addition, investigating the intricacies of the spectral effects can provide interpretable a priori knowledge for advanced methods such as deep learning.

In our future research, we will also consider employing more advanced and fault-sensitive frequency analysis methods to replace FFT, as well as more sophisticated data preprocessing techniques such as noise reduction and feature enhancement. These will be utilized to enhance the CM and early anomaly detection capabilities of the SPCA method. The resulting characteristic frequency components will then be integrated with advanced diagnostic methods for application in high-precision diagnostics.

REFERENCES

[1] G. W. Vogl, B. A. Weiss, and M. Helu, "A review of diagnostic and prognostic capabilities and best practices for manufacturing," *J. Intell. Manuf.*, vol. 30, no. 1, pp. 79–95, Jan. 2019, doi: 10.1007/s10845-016-1228-8.

[2] H. Meng and Y.-F. Li, "A review on prognostics and health management (PHM) methods of lithium-ion batteries," *Renew. Sustain. Energy Rev.*, vol. 116, Dec. 2019, Art. no. 109405, doi: 10.1016/j.rser.2019.109405.

[3] M. Kordestani, M. E. Orchard, K. Khorasani, and M. Saif, "An overview of the state of the art in aircraft prognostic and health management strategies," *IEEE Trans. Instrum. Meas.*, vol. 72, pp. 1–15, 2023, doi: 10.1109/TIM.2023.3236342.

[4] J. Lee, F. J. Wu, W. Y. Zhao, M. Ghaffari, L. X. Liao, and D. Siegel, "Prognostics and health management design for rotary machinery systems-reviews, methodology and applications," *Mech. Syst. Signal Process.*, vol. 42, nos. 1–2, pp. 314–334, Jan. 2014, doi: 10.1016/j.ymssp.2013.06.004.

[5] B. Rezaeianjouybari and Y. Shang, "Deep learning for prognostics and health management: State of the art, challenges, and opportunities," *Measurement*, vol. 163, Oct. 2020, Art. no. 107929, doi: 10.1016/j.measurement.2020.107929.

[6] Y. Lei, J. Lin, M. J. Zuo, and Z. He, "Condition monitoring and fault diagnosis of planetary gearboxes: A review," *Measurement*, vol. 48, pp. 292–305, Feb. 2014, doi: 10.1016/j.measurement.2013.11.012.

[7] H. D. M. de Azevedo, A. M. Araújo, and N. Bouchonneau, "A review of wind turbine bearing condition monitoring: State of the art and challenges," *Renew. Sustain. Energy Rev.*, vol. 56, pp. 368–379, Apr. 2016, doi: 10.1016/j.rser.2015.11.032.

[8] S. A. Aburakhia, R. Myers, and A. Shami, "A hybrid method for condition monitoring and fault diagnosis of rolling bearings with low system delay," *IEEE Trans. Instrum. Meas.*, vol. 71, pp. 1–13, 2022, doi: 10.1109/TIM.2022.3198477.

[9] O. AlShorman et al., "Sounds and acoustic emission-based early fault diagnosis of induction motor: A review study," *Adv. Mech. Eng.*, vol. 13, no. 2, Feb. 2021, Art. no. 168781402199691, doi: 10.1177/1687814021996915.

[10] Y. Lei, N. Li, L. Guo, N. Li, T. Yan, and J. Lin, "Machinery health prognostics: A systematic review from data acquisition to RUL prediction," *Mech. Syst. Signal Process.*, vol. 104, pp. 799–834, May 2018, doi: 10.1016/j.ymssp.2017.11.016.

[11] C. Hu, B. D. Youn, P. Wang, and J. Taek Yoon, "Ensemble of data-driven prognostic algorithms for robust prediction of remaining useful life," *Rel. Eng. Syst. Saf.*, vol. 103, pp. 120–135, Jul. 2012, doi: 10.1016/j.ress.2012.03.008.

[12] N. Li, Y. Lei, J. Lin, and S. X. Ding, "An improved exponential model for predicting remaining useful life of rolling element bearings," *IEEE Trans. Ind. Electron.*, vol. 62, no. 12, pp. 7762–7773, Dec. 2015, doi: 10.1109/TIE.2015.2455055.

[13] A. Malhi, R. Yan, and R. X. Gao, "Prognosis of defect propagation based on recurrent neural networks," *IEEE Trans. Instrum. Meas.*, vol. 60, no. 3, pp. 703–711, Mar. 2011, doi: 10.1109/TIM.2010.2078296.

[14] R. B. Randall and J. Antoni, "Rolling element bearing diagnostics—A tutorial," *Mech. Syst. Signal Process.*, vol. 25, no. 2, pp. 485–520, Feb. 2011, doi: 10.1016/j.ymssp.2010.07.017.

[15] J. Antoni, "The spectral kurtosis: A useful tool for characterising non-stationary signals," *Mech. Syst. Signal Process.*, vol. 20, no. 2, pp. 282–307, Feb. 2006, doi: 10.1016/j.ymssp.2004.09.001.

[16] J. Antoni and R. B. Randall, "The spectral kurtosis: Application to the vibratory surveillance and diagnostics of rotating machines," *Mech. Syst. Signal Process.*, vol. 20, no. 2, pp. 308–331, Feb. 2006, doi: 10.1016/j.ymssp.2004.09.002.

[17] J. Antoni, "Fast computation of the Kurtogram for the detection of transient faults," *Mech. Syst. Signal Process.*, vol. 21, no. 1, pp. 108–124, Jan. 2007, doi: 10.1016/j.ymssp.2005.12.002.

[18] I. S. Bozchalooi and M. Liang, "A smoothness index-guided approach to wavelet parameter selection in signal de-noising and fault detection," *J. Sound Vib.*, vol. 308, nos. 1–2, pp. 246–267, Nov. 2007, doi: 10.1016/j.jsv.2007.07.038.

[19] J. Antoni, "The infogram: Entropic evidence of the signature of repetitive transients," *Mech. Syst. Signal Process.*, vol. 74, pp. 73–94, Jun. 2016, doi: 10.1016/j.ymssp.2015.04.034.

[20] Y. Miao, M. Zhao, and J. Lin, "Improvement of kurtosis-guided-grams via Gini index for bearing fault feature identification," *Meas. Sci. Technol.*, vol. 28, no. 12, Dec. 2017, Art. no. 125001, doi: 10.1088/1361-6501/aa8a57.

[21] D. Wang, Z. Peng, and L. Xi, "The sum of weighted normalized square envelope: A unified framework for kurtosis, negative entropy, Gini index and smoothness index for machine health monitoring," *Mech. Syst. Signal Process.*, vol. 140, Jun. 2020, Art. no. 106725, doi: 10.1016/j.ymssp.2020.106725.

[22] B. Hou, D. Wang, J.-Z. Kong, J. Liu, Z. Peng, and K.-L. Tsui, "Understanding importance of positive and negative signs of optimized weights used in the sum of weighted normalized Fourier spectrum/envelope spectrum for machine condition monitoring," *Mech. Syst. Signal Process.*, vol. 174, Jul. 2022, Art. no. 109094, doi: 10.1016/j.ymssp.2022.109094.

[23] Q. Miao, H.-Z. Huang, and X. Fan, "Singularity detection in machinery health monitoring using Lipschitz exponent function," *J. Mech. Sci. Technol.*, vol. 21, no. 5, pp. 737–744, May 2007, doi: 10.1007/bf02916351.

[24] J. Antoni and P. Borghesani, "A statistical methodology for the design of condition indicators," *Mech. Syst. Signal Process.*, vol. 114, pp. 290–327, Jan. 2019, doi: 10.1016/j.ymssp.2018.05.012.

[25] J. Antoni et al., "On the design of optimal health indicators for early fault detection and their statistical thresholds," *Mech. Syst. Signal Process.*, vol. 218, Sep. 2024, Art. no. 111518, doi: 10.1016/j.ymssp.2024.111518.

[26] L. Guo, N. Li, F. Jia, Y. Lei, and J. Lin, "A recurrent neural network based health indicator for remaining useful life prediction of bearings," *Neurocomputing*, vol. 240, pp. 98–109, May 2017, doi: 10.1016/j.neucom.2017.02.045.

[27] H. Ocak, K. A. Loparo, and F. M. Discenzo, "Online tracking of bearing wear using wavelet packet decomposition and probabilistic modeling: A method for bearing prognostics," *J. Sound Vibrat.*, vol. 302, nos. 4–5, pp. 951–961, May 2007, doi: 10.1016/j.jsv.2007.01.001.

[28] D. Wang, Q. Miao, Q. Zhou, and G. Zhou, "An intelligent prognostic system for gear performance degradation assessment and remaining useful life estimation," *J. Vibrat. Acoust.*, vol. 137, no. 2, Apr. 2015, Art. no. 021004, doi: 10.1115/1.4028833.

[29] S. Zhang, Y. Zhang, L. Li, and J. Zhu, "Rolling elements bearings degradation indicator based on continuous hidden Markov model," *J. Failure Anal. Prevention*, vol. 15, no. 5, pp. 691–696, Oct. 2015, doi: 10.1007/s11668-015-9999-3.

[30] S. A. Aye, P. S. Heyns, and C. J. H. Thiart, "Fault detection of slow speed bearings using an integrated approach," *IFAC-PapersOnLine*, vol. 48, no. 3, pp. 1779–1784, 2015, doi: 10.1016/j.ifacol.2015.06.344.

[31] S. Dong and T. Luo, "Bearing degradation process prediction based on the PCA and optimized LS-SVM model," *Measurement*, vol. 46, no. 9, pp. 3143–3152, Nov. 2013, doi: 10.1016/j.measurement.2013.06.038.

[32] A. Widodo and B.-S. Yang, "Application of relevance vector machine and survival probability to machine degradation assessment," *Exp. Syst. Appl.*, vol. 38, no. 3, pp. 2592–2599, Mar. 2011, doi: 10.1016/j.eswa.2010.08.049.

[33] J. Wu, C. Wu, S. Cao, S. W. Or, C. Deng, and X. Shao, "Degradation data-driven time-to-failure prognostics approach for rolling element bearings in electrical machines," *IEEE Trans. Ind. Electron.*, vol. 66, no. 1, pp. 529–539, Jan. 2019, doi: 10.1109/TIE.2018.2811366.

[34] Q. He, R. Yan, F. Kong, and R. Du, "Machine condition monitoring using principal component representations," *Mech. Syst. Signal Process.*, vol. 23, no. 2, pp. 446–466, Feb. 2009, doi: 10.1016/j.ymssp.2008.03.010.

[35] Q. He, F. Kong, and R. Yan, "Subspace-based gearbox condition monitoring by kernel principal component analysis," *Mech. Syst. Signal Process.*, vol. 21, no. 4, pp. 1755–1772, May 2007, doi: 10.1016/j.ymssp.2006.07.014.

[36] V. H. Nguyen and J.-C. Golinval, "Fault detection based on kernel principal component analysis," *Eng. Struct.*, vol. 32, no. 11, pp. 3683–3691, 2010, doi: 10.1016/j.engstruct.2010.08.012.

[37] J. Zhang, D. Zhou, and M. Chen, "Self-learning sparse PCA for multimode process monitoring," *IEEE Trans. Ind. Informat.*, vol. 19, no. 1, pp. 29–39, Jan. 2023, doi: 10.1109/TII.2022.3178736.

[38] P. Ma, J. Ren, H. Zhao, G. Sun, P. Murray, and J. Zheng, "Multiscale 2-D singular spectrum analysis and principal component analysis for spatial–spectral noise-robust feature extraction and classification of hyperspectral images," *IEEE J. Sel. Topics Appl. Earth Observ. Remote Sens.*, vol. 14, pp. 1233–1245, 2021, doi: 10.1109/JSTARS.2020.3040699.

[39] J. Zabalza et al., "Novel two-dimensional singular spectrum analysis for effective feature extraction and data classification in hyperspectral imaging," *IEEE Trans. Geosci. Remote Sens.*, vol. 53, no. 8, pp. 4418–4433, Aug. 2015, doi: 10.1109/TGRS.2015.2398468.

[40] T. Yan, D. Wang, T. Xia, J. Liu, Z. Peng, and L. Xi, "Investigation on optimal discriminant directions of linear discriminant analysis for locating informative frequency bands for machine health monitoring," *Mech. Syst. Signal Process.*, vol. 180, Nov. 2022, Art. no. 109424, doi: 10.1016/j.ymssp.2022.109424.

[41] P. Borghesani, W. A. Smith, R. B. Randall, J. Antoni, M. El Badaoui, and Z. Peng, "Bearing signal models and their effect on bearing diagnostics," *Mech. Syst. Signal Process.*, vol. 174, Jul. 2022, Art. no. 109077, doi: 10.1016/j.ymssp.2022.109077.

[42] H. Qiu, J. Lee, J. Lin, and G. Yu, "Wavelet filter-based weak signature detection method and its application on rolling element bearing prognostics," *J. Sound Vibrat.*, vol. 289, nos. 4–5, pp. 1066–1090, Feb. 2006, doi: 10.1016/j.jsv.2005.03.007.

[43] W. Gousseau, J. Antoni, F. Girardin, U. Lyon, and J. Griffaton, "Analysis of the rolling element bearing data set of the center for intelligent maintenance systems of the University of Cincinnati," in *Proc. CM*, 2016, pp. 1–14.

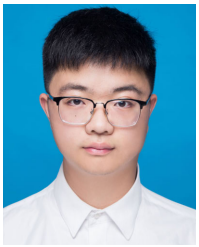

Yingchun Li received the B.S. degree from the School of Mechanical Engineering, Hefei University of Technology, Hefei, China, in 2022. He is currently pursuing the master's degree in mechanical engineering from the Department of Mechanical Engineering, Xi'an Jiaotong University, Xi'an, China.

His current research interests are focused on condition monitoring, anomaly detection, machine learning, and fault diagnosis.

Yu Sun (Member, IEEE) received the B.S. degree from the School of Mechanical Engineering, Northwestern Polytechnical University, Xi'an, China, in 2007, and the Ph.D. degree from the University of Tokyo, Tokyo, Japan, in 2012.

She is currently an Associate Professor with the School of Mechanical Engineering, Xi'an Jiaotong University, Xi'an. Her research interests include structural health monitoring, intelligent sensing and multiscale design, and soft robotics.

Zhiyuan Li received the B.S. degree in mechanical and electrical engineering from Xi'an Polytechnic University, Xi'an, China, in 2020, and the M.S. degree in mechanical engineering from the Department of Mechanical Engineering, Xi'an Jiaotong University, Xi'an, in 2023.

He is currently working as an Assistant Engineer with CREEC (Chongqing) Survey Design and Research Company Ltd., Chongqing, China.

Xuefeng Chen (Senior Member, IEEE) received the Ph.D. degree in mechanical engineering from Xi'an Jiaotong University, Xi'an, China, in 2004.

He is currently a Professor of mechanical engineering with Xi'an Jiaotong University. His current research interests include finite-element methods, mechanical system and signal processing, diagnosis and prognosis for complicated industrial systems, smart structures, aeroengine fault diagnosis, and wind turbine system monitoring.

Laihao Yang (Member, IEEE) received the B.S. and Ph.D. degrees from the School of Mechanical Engineering, Xi'an Jiaotong University, Xi'an, China, in 2013 and 2019, respectively.

He was a Research Fellow with the Structural Dynamics and Acoustic Systems Laboratory (SDASL), University of Massachusetts (US), Amherst, MA, USA, from 2018 to 2019. He is now an Assistant Professor with the School of Mechanical Engineering, Xi'an Jiaotong University. He has published over 30 refereed journal and conference publications and presented over five oral presentations at international congresses and conferences. His research interests include nonlinear vibration modeling and analysis, data-driven dynamic modeling, compressive sensing, interpretable AI, and soft robotics.